Frontiers in Heat and Mass Transfer (FHMT), 4, 023004 (2013)
DOI: 10.5098/hmt.v4.2.3004

Global Digital Central
ISSN: 2151-8629

Frontiers in Heat and Mass Transfer

Available at www.ThermalFluidsCentral.org

ANALYSIS OF CHAOTIC NATURAL CONVECTION IN A TALL RECTANGULAR CAVITY WITH NON-ISOTHERMAL WALLS

Heather Dillon[a], Ashley Emery[b,†], Ann Mescher[b]

[a]*Dept of Mechanical Engineering, University of Portland, Portland, Oregon, 97203, USA*
[b]*Dept of Mechanical Engineering, University of Washington, Seattle, Washington, 98105, USA*

ABSTRACT

A computational model is presented that extends prior work on unsteady natural convection in a tall rectangular cavity with aspect ratio 10 and applies Proper Orthogonal Decomposition to the results. The solution to the weakly compressible Navier-Stokes equation is computed for a range of Rayleigh numbers between 2×10^7 and 2.2×10^8 with Prandtl number 0.71. A detailed spectral analysis shows dynamic system behavior beyond the Hopf bifurcation that was not previously observed. The wider Rayleigh range reveals new dynamic system behavior for the rectangular geometry, specifically a return to a stable oscillatory behavior that was not predicted in prior work. Proper Orthogonal Decomposition (POD) has been used to analyze the computational results. Five eigenvalue modes were required to capture correctly the basic flow structure. The POD failed to capture subtle aspects of the flow structure at high Rayleigh numbers for the model, indicating that a POD and Galerkin projection for several Rayleigh numbers will be needed to reproduce the complex behavior of the system.

Keywords: *Proper Orthogonal Decomposition, natural convection, reduced order modeling, computational fluid dynamics*

1. INTRODUCTION

Natural convection in a tall cavity with non-isothermal vertical walls has many applications including optical fiber manufacturing, optimizing computer component locations, and composite building walls. Computational work has explored a wide variety of boundary conditions, however the case of non-uniform wall temperatures has only been explored by a small group.

For the case of isothermal walls in tall cavities the flow will transition from the conduction regime to the convection regime at the critical Rayleigh number (Ra_c). As the Rayleigh number (Ra) is further increased, the system will transition to chaotic behavior. The chaotic behavior of the system has been shown to exhibit hysteresis, intermittency, a supercritical Hopf bifurcation, and period doubling. Several parameters are used to classify the systems. The geometry of the cavity is represented by the aspect ratio (A), where $A = H/W$. H is the height of the cavity and W is the width.

Convection in a tall cavity has been studied by many authors in the last 30 years as summarized in Table 1. The work of Reeve *et al.* (2004) is the only prior work to consider the same boundary conditions as in the present work. Here, the range of Rayleigh numbers has been extended. The boundary conditions for the system are specified as adiabatic on the upper and lower cavity boundaries as shown in Figure 1. The temperature on the right and left walls are constrained to vary linearly in the y-direction as shown in Figure 2. Reeve *et al.* (2004) observed that these boundary conditions, at low Rayleigh number, create a steady bi-cellular flow in contrast to uni-cellular flow for isothermal vertical walls.

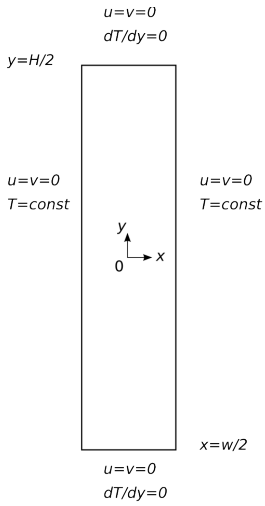

Fig. 1 Schematic of the computational domain.

All of the authors summarized in Table 1 considered isothermal vertical walls except Reeve *et al.* (2004). Some authors (Paolucci and Chenoweth (1989) and Haldenwang and Labrosse (1986)) predict an oscillatory instability for tall cavities. Chenoweth and Paolucci (1996) observed that as the temperature difference in the cavity is increased, a

[†]*Corresponding author. Email: emery@u.washington.edu*

Global Digital Central
ISSN: 2151-8629

Table 1 Summary of computational work for rectangular natural convection systems.

Author	Year	Ra	Pr	A	Description
Vest and Arpaci (1969)	1969	$7 \times 10^3 - 3 \times 10^5$	0.71, 1000	20-33	Galerkin method.
Korpela *et al.* (1973)	1973	$1 \times 10^2 - 1 \times 10^4$	0-50	∞	Report Ra_c as a function.
Lee and Korpela (1983)	1983	$3 \times 10^4 - 2 \times 10^5$	0-1000	15-40	Report Nusselt and streamfunctions.
Chenoweth and Paolucci (1996)	1986	$1 \times 10^5 - 1 \times 10^6$	0.71	1-10	Compare ideal gas and Boussinesq.
Chait and Korpela (1989)	1989	$5 \times 10^2 - 1.5 \times 10^4$	0.71, 1000	∞	Pseudospectral method. Reported Ra_c.
Paolucci and Chenoweth (1989)	1989		0.71	0.5-3	Frequency results, bifurcation and phase diagrams.
LeQuere (1990)	1990	$7 \times 10^3 - 4 \times 10^4$	0.71	16	Explored return to uni-cellular pattern.
Liakopoulos *et al.* (1990)	1990		0.71	10-25	Included flux wall conditions.
Suslov and Paolucci (1995)	1995	$6 \times 10^3 - 1 \times 10^4$	0.71	∞	Non-Boussinesq impact on stability and considered Ra_c with ΔT.
Xin and LeQuere (2002)	2002	$3 \times 10^5 - 5 \times 10^5$	0.71	8	Benchmark study reports Ra_c.
Reeve (2003)	2003	$2 \times 10^7 - 1 \times 10^8$	0.71	10	Commercial code FIDAP.

lower critical Rayleigh number is found. Related work in annular geometries has been explored in prior work experiementally and compuationally (Dillon *et al.*, 2011b). Early computational results for the geometry considered are presented in Dillon *et al.* (2011a) and extended with reduced order analysis in this paper.

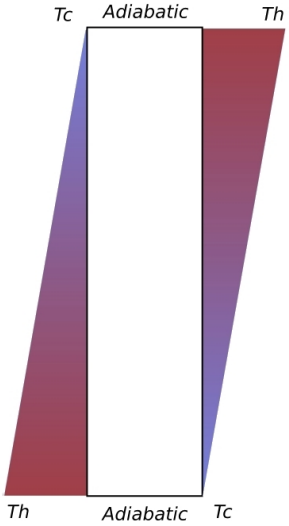

Fig. 2 Linear temperature profile boundary conditions applied to the vertical walls of the cavity.

2. METHODS

This problem was analyzed using a traditional computational tools like COMSOL and an analysis technique called proper orthogonal decomposition.

2.1. Computational Tool

The computational tool COMSOL was used to perform the simulations. Prior to this investigation the computational tool was benchmarked with experimental results from the literature, specifically Vest and Arpaci (1969), and compared to other models (Lee and Korpela (1983), Liakopoulos *et al.* (1990), Xin and LeQuere (2002), Reeve (2003)). The benchmarking work is documented in Dillon (2011).

The buoyancy driven flow is modeled as a coupled system with fluid motion (Navier-Stokes) and heat transfer. The model equations are given in Equations 1-3.

In this form u represents the velocity vector of the fluid, ρ is the fluid density, μ is the dynamic viscosity of the fluid, and f is the body force applied to the fluid. The heat transfer is governed by Equation 3. For this equation k is the thermal conductivity, c_p is the specific heat at constant pressure, and T is the temperature.

$$\rho\frac{\partial u}{\partial t} + \rho(u \cdot \bigtriangledown)u = \bigtriangledown \cdot (-pI + \mu(\bigtriangledown u + \bigtriangledown u^T) - (2\mu/3 \cdot \bigtriangledown \cdot u)I) + f \quad (1)$$

$$\frac{\partial \rho}{\partial t} + \bigtriangledown \cdot (\rho u) = 0 \quad (2)$$

$$\rho c_p \frac{\partial T}{\partial t} + \bigtriangledown \cdot (-k \bigtriangledown T) = -\rho c_p u \cdot \bigtriangledown T \quad (3)$$

The boundary conditions for the system are specified as no slip and adiabatic on the upper and lower cavity boundaries. The right and left wall temperatures have a linear profile given by $T(y) = T_h \cdot (1 - y)$ and $T(y) = T_c \cdot y$.

A grid resolution study was conducted to determine the required mesh density and to compare the results with those computed by Reeve *et al.* (2004) using FIDAP. Results for a 1120 element triangular mesh were consistent with the results of Reeve and this triangular mesh was used for computations. This is documented in more detail in Dillon (2011) and Dillon *et al.* (2009).

The density of the fluid is represented with the Boussinesq approximation to simplify the formation of the coupled Navier-Stokes equations. The height of the cavity H is the characteristic length and the temperature difference between T_h and T_c is the characteristic temperature, $\Delta T = (T_h - T_c)$. From this the dimensionless temperature becomes $\Theta = (T - T_c)/(\Delta T)$. The dimensionless time is $\tau = t\sqrt{g\beta\Delta T H^{-1}}$. The dimensionless velocity was chosen based on the work of Reeve *et al.* (2004) as $u/\sqrt{g\beta\Delta T H}$. Aspects of the dimensionless parameters are discussed in more detail in Dillon *et al.* (2010) and Dillon (2011).

2.2. Proper Orthogonal Decomposition

Proper Orthogonal Decomposition (POD) is based on the diagonalization of a matrix. The mathematical procedure linearly transforms the number of possibly correlated variables into a smaller number of uncorrelated variables. The first component contains as much of the variation in the system as possible. Assume a matrix X is an $m \times n$ matrix composed of multiple observations from a simulation.

For the POD analysis the data is centered by the mean of each row. Then the covariance matrix Cx is calculated. The covariance matrix is a square, symmetric $m \times m$ matrix whose diagonal represents the variance of particular measurements. Small diagonal terms indicate the variables are statistically independent.

Global Digital Central
ISSN: 2151-8629

$$C_x = \frac{1}{n-1} X X^T \tag{4}$$

Singular Value Decomposition (SVD) is used to diagonalize the matrix. The SVD diagonalization is shown in Equation 5, where $U \in \mathbb{C}^{m\times m}$ is unitary, $V \in \mathbb{C}^{n\times n}$ is unitary, and $\Sigma \in \mathbb{R}^{m\times n}$ is diagonal. If full SVD is used for calculations it may be applied to rank deficient matrices as described by Trefethen and Bau (1997).

$$X = U\Sigma V^* \tag{5}$$

V^* is the hermitian conjugate or adjoint of the matrix V. This means that the complex conjugate of each entry in the matrix is calculated and then the matrix is transposed.

> **Theorem:** Every matrix $X \in \mathbb{C}^{m\times n}$ has a singular value decomposition. Furthermore, the singular values $\{\sigma_j\}$ are uniquely determined, and if X is square and the σ_j distinct, the singular vectors $\{u_j\}$ and $\{v_j\}$ are uniquely determined up to complex signs (complex scalar factors of absolute value 1) as described by Trefethen and Bau (1997).

A visual representation of the SVD process is shown in Figure 3. The following theorems Trefethen and Bau (1997) illustrate the way SVD is linked to POD, where the first confirms that the basis vectors are unique and the second theorem allows determination of N such that the Nth partial sum captures as much of matrix X as possible.

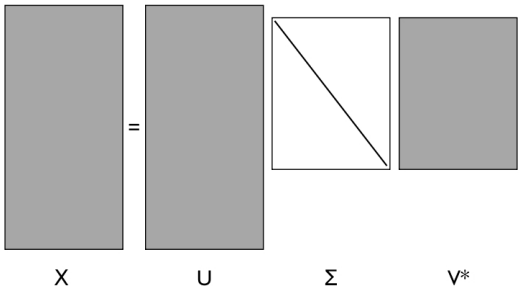

Fig. 3 Visual representation of the SVD diagonalization. Adapted from Trefethen and Bau (1997).

> **Theorem:** X is the sum of r rank-one matrices.
>
> $$X = \Sigma_{j=1}^{r} \sigma_r u_j v_j^* \tag{6}$$
>
> **Theorem:** For any N such that $0 \leq N \leq r$, we can define the partial sum
>
> $$X = \Sigma_{j=1}^{N} \sigma_r u_j v_j^*$$
>
> And if $N = min\{m, n\}$, define $\sigma_{N+1} = 0$. Then
>
> $$\|X - X_N\|_2 = \sigma_{N+1}$$

The SVD gives a type of least-square fitting algorithm, allowing us to project the matrix onto low-dimensional representations in a formal, algorithmic way as shown by Trefethen and Bau (1997). The matrix may also be projected onto other basis as considered by other authors in the literature. For this work, the matrix is projected back onto the data to investigate the contribution of each mode to the observed data to augment the frequency analysis.

2.3. Galerkin Projection

Many authors use the POD to build more elaborate models based on the calculated modes. The most common is a Galerkin projection, but some authors explored alternatives like Method of Polyargumental Systems (MPS), Blinov *et al.* (2004), Linear Stochastic Estimation (LSE), Bonnet *et al.* (1994), Equation Free (EF) modeling, Sirisup *et al.* (2005), and balanced truncation, Rowley (2005); Rowley and Marsden (2000).

For transient natural convection the Galerkin projection has been used frequently. The formulation of the Galerkin projection for natural convection problems is based on the Boussinesq equations. The Galerkin method is used to simplify the equations to a set of non-linear ordinary differential equations based on the orthogonal nature of the POD.

If $\hat{U}$ is the vector of the radial and axial velocities the Boussinesq approximation may be expressed in terms of the Grashof number (Gr) and the Prandlt number (Pr).

$$\frac{\partial \hat{U}}{\partial t} + (\hat{U}\cdot\nabla)\hat{U} + \nabla P = \Theta + \frac{1}{\sqrt{Gr}}\nabla^2\hat{U} \tag{7}$$

$$\frac{\partial \Theta}{\partial t} + \hat{U}\cdot\nabla\Theta = \frac{1}{Pr\sqrt{Gr}}\nabla^2\Theta \tag{8}$$

$$\nabla\cdot\hat{U} = 0 \tag{9}$$

Using the derivation of Liakopoulos *et al.* (1997), the stationary empirical eigenfunctions for the temperature (ϕ_k) and flow field (φ_k) are determined for a specific Gr and Pr, (equivalent to a specific Ra) using POD. The input temperature (Θ) and flow field $(\hat{U})$ are separated into time varying $(\Theta', \hat{U}')$ part and time averaged components prior to performing the POD, and can then be expanded in terms of the calculated eigenfunctions.

$$\hat{U}' = \sum_{k=1}^{M} a_k(t)\varphi_k \tag{10}$$

$$\Theta' = \sum_{k=1}^{M} b_k(t)\phi_k \tag{11}$$

The expansion coefficients (a_k, b_k) are calculated via integration over the spatial domain from the known eigenfunctions.

$$\begin{aligned} a_k(t) &= \int\int \hat{U}'\cdot\varphi_k d\Omega \quad k = 1, 2, ..., M \\ b_k(t) &= \int\int \Theta'\cdot\phi_k d\Omega \quad k = 1, 2, ..., M \end{aligned} \tag{12}$$

Substitution of the expansion coefficients into the Boussinesq equations provides a simplified model for the system based on a set of coefficients $(A_k, B_k, C_k, ...K_k)$ for $k = 1, 2, ..., M$ which are determined from inner products of the eigenfunctions and the flow properties.

$$\frac{da_k}{dt} = A_k + \frac{1}{\sqrt{Gr}}B_k + C_{ki}a_i + \frac{1}{\sqrt{Gr}}D_{ki}a_i + E_{kij}a_i a_j + R_{ki}b_i \tag{13}$$

$$\frac{db_k}{dt} = F_k + \frac{1}{Pr\sqrt{Gr}}G_k + H_{ki}a_i + \frac{1}{Pr\sqrt{Gr}}I_{ki}b_i + J_{kij}a_i b_j + K_{ki}b_i \tag{14}$$

This set of equations has been used by authors to represent the flow and explore the dynamic system properties. The key limitation to this approach is the restriction of the POD to a calculation at one specific Rayleigh number. The exploration of the flow near that Rayleigh number is likely to be well captured by the set of derived equations, but accurate representation of the system using the simplified expressions over a large range of Rayleigh numbers is unlikely.

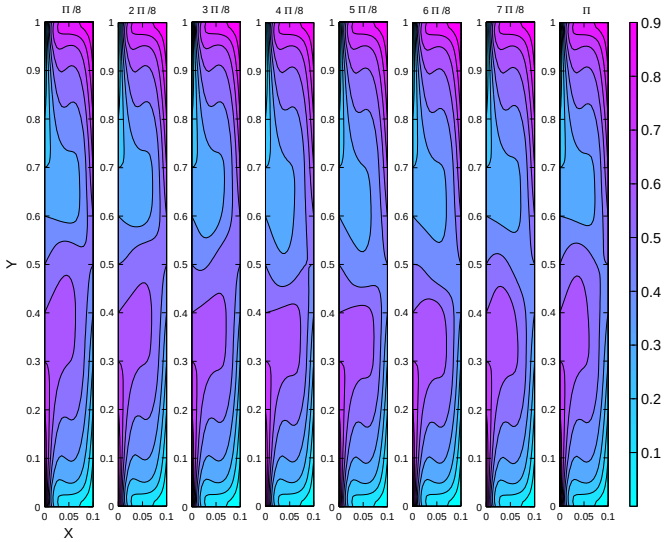

(a) Θ

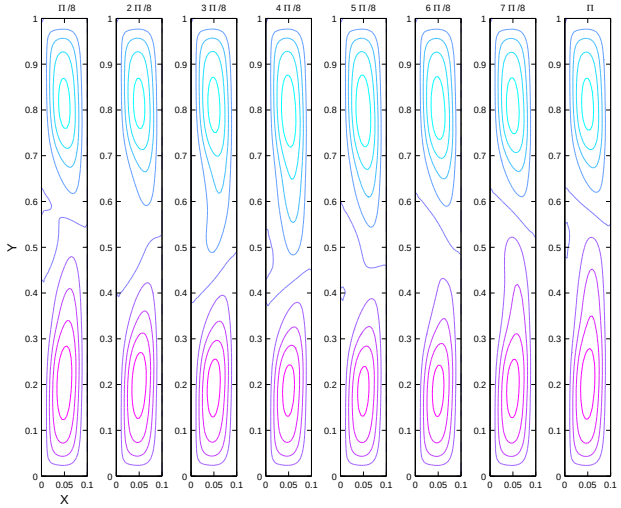

(b) ψ

Fig. 4 Sequential contour plot of the temperature Θ (upper) and stream function ψ (lower) for the rectangular cavity illustrating oscillation of the natural convection cells through one period (Π). $Ra = 2.5 \times 10^7$, $A = 10$.

3. COMPUTATIONAL RESULTS

For the rectangular cavity, the results for Rayleigh number below $Ra = 1.0 \times 10^8$ are consistent with the results from Reeve. A transition from steady to oscillatory flow is observed at $Ra = 2.2 \times 10^7$ as the system undergoes a supercritical Hopf bifurcation. Figure 4 shows one period of oscillations at $Ra = 2.5 \times 10^7$, after the bifurcation results in oscillatory flow. A second transition from oscillatory to chaotic flow is observed at $Ra = 4.5 \times 10^7$.

In the rectangular cavity as the Rayleigh number is increased the frequency of the oscillations increases. Figure 5 shows the amplitude of the temperature oscillations at the center of the cavity at several Rayleigh numbers. The local region of the oscillations near the center of the cavity also becomes smaller as the the Rayleigh number increases.

A second, unexpected, transition back to oscillatory flow is predicted at $Ra = 1.27 \times 10^8$. Figure 9 shows one period of oscillations for $Ra = 1.7 \times 10^8$ where the behavior is again oscillatory with a third cell

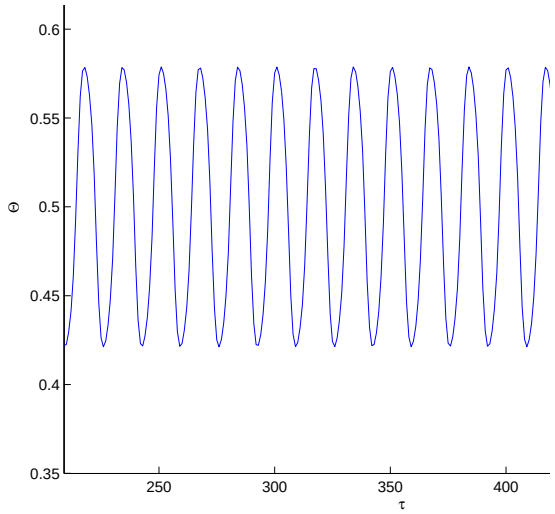

(a) $Ra = 2.5 \times 10^7$

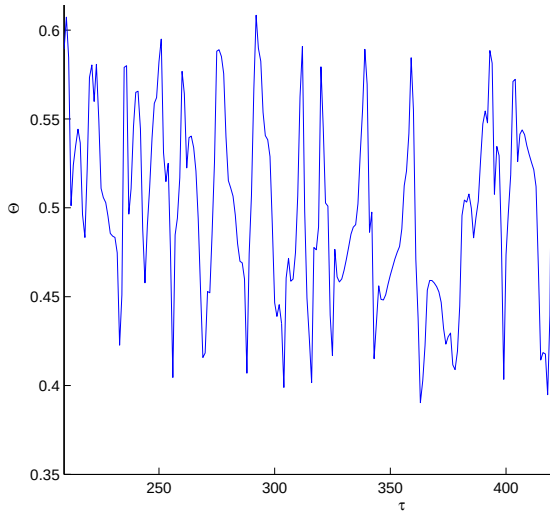

(b) $Ra = 10 \times 10^7$

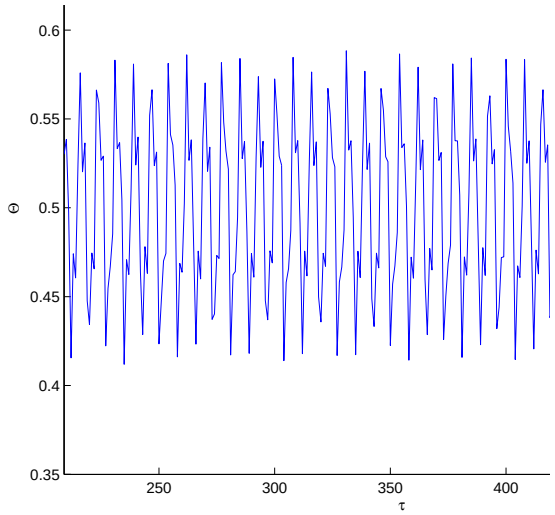

(c) $Ra = 17 \times 10^7$

Fig. 5 Temperature oscillations in the center of the cavity for $A = 10$ showing the increase in the frequency of the oscillations and the effect of the harmonics in the oscillations.

formation near the center of the cavity. In Reeve's previous research of the rectangular geometry, a tri-cellular solution path was not predicted; however, Reeve observed a similar phenomena at high Rayleigh numbers in an annular cavity.

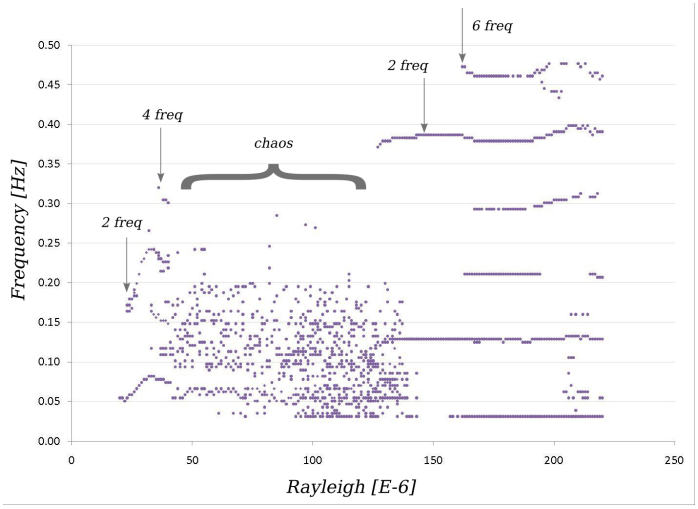

Fig. 6 Frequency summary of the temperature oscillations in the center of the rectangular cavity, $A = 10$ (listing the number of frequencies observed).

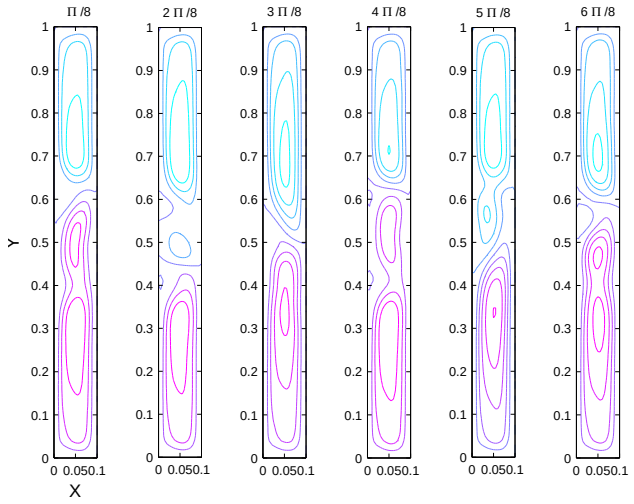

Fig. 7 Sequential contour plot of the stream function for the rectangular cavity illustrating oscillation of the natural convection cells through one period (Π) in the chaotic region. $Ra = 10 \times 10^7$, $A = 10$.

The most interesting aspects of the solution are visible when the the full frequency spectrum is shown. The peak frequencies were calculated and are shown in Figure 6. The frequency analysis reveals that the lower frequency (near 0.05 Hz) has more power than the higher frequencies in the oscillations. The initial transition to chaotic behavior is observed to occur via period halving, where two frequencies are first seen at 0.051 Hz and 0.164 Hz ($Ra = 2.2{\times}10^7$). Then at $Ra = 3.6{\times}10^7$ four frequencies are visible at 0.078, 0.160, 0.238 and 0.320 Hz. The transition to chaotic behavior at $Ra = 4.5 \times 10^7$ is shown by a collection of frequencies in the spectrum. This region ends abruptly at $Ra = 13.8 \times 10^7$ with the appearance of two frequencies at 0.129 and 0.371 Hz. The frequencies may exhibit period doubling but the Rayleigh number resolution does not show a second bifurcation, rather the system jumps to six frequencies at

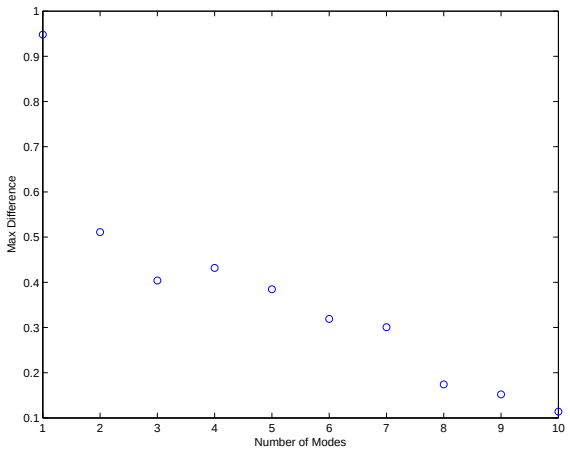

(a) POD Θ

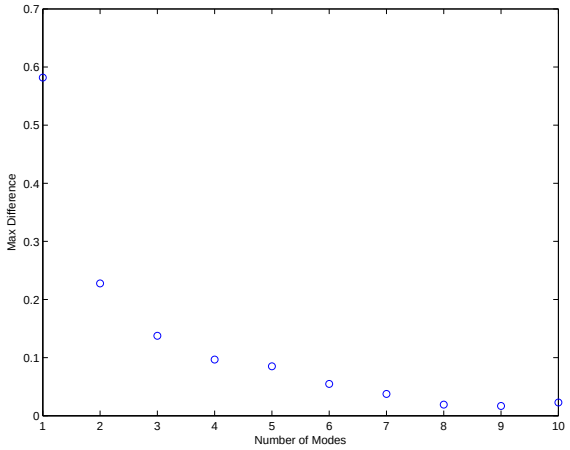

(b) POD ψ

Fig. 8 Temperature (a) and streamfunction (b) maximum difference between the POD and original solution for $Ra = 17 \times 10^7$.

$Ra = 16.3 \times 10^7$. The highest frequency (0.465 Hz) bifurcates again at $Ra = 19.3 \times 10^7$ as shown in the upper right of Figure 6.

The nature of the chaotic behavior is dominated by the formation of the third cell in the cavity. Figure 7 shows an example of behavior in the chaotic region ($Ra = 10 \times 10^7$). The center region of the cavity experiences chaotic temperatures and velocities but the upper and lower regions of the cavity remain relatively stable. Eventually, at higher Rayleigh number, the third cell stabilizes as shown in Figure 4 with six frequencies in the system.

4. POD RESULTS

To quantify the dynamic behavior of the system Proper Orthogonal Decomposition (POD) was applied to the temperature and velocity field of the simulation solution set. At specific Rayleigh numbers the time dependent velocity streamfunction (ψ) and temperature (Θ) data are used to calculate stationary empirical eigenfunctions (modes). The modes are determined from M snapshots representing at least four periods of oscillation based on the technique of Sirovich (1987).

Global Digital Central
ISSN: 2151-8629

Table 2 Summary of modes and energy for the POD. Eigenvalues for the five most energetic modes and the contribution to the system energy at $Ra = 2.5 \times 10^7$ and $Ra = 17 \times 10^7$ in the rectangular cavity.

$Ra = 2.5 \times 10^7$	**Temperature**	**Eigenvalues**	**Streamfunction**	**Eigenvalues**
Mode	**eigenvalue** σ	**Total Energy** *percent*	**eigenvalue** σ	**Total Energy** *percent*
1	0.59292	47.0954	0.012625	38.4593
2	0.34788	68.9592	0.0047368	76.9099
3	0.07136	93.6327	0.0018725	90.8724
4	0.056986	94.9153	0.00077265	96.2336
5	0.024877	97.7803	0.00024232	98.8188
$Ra = 17 \times 10^7$	**Temperature**	**Eigenvalues**	**Streamfunction**	**Eigenvalues**
Mode	**eigenvalue** σ	**Total Energy** *percent*	**eigenvalue** σ	**Total Energy** *percent*
1	0.71757	68.2151	0.029221	51.1865
2	0.57901	74.3525	0.015352	74.3544
3	0.22331	90.1084	0.0063467	89.3977
4	0.19776	91.2402	0.003891	93.5001
5	0.13517	94.0127	0.0015179	97.4643

$$X = \begin{bmatrix} \Theta_{1,1}(t_1) & \Theta_{1,2}(t_1) & \dots \\ \Theta_{1,1}(t_2) & \Theta_{1,2}(t_2) & \dots \\ \vdots & & \vdots \\ \Theta_{1,1}(t_m) & \Theta_{1,2}(t_m) & \dots \end{bmatrix}$$

The eigenvalues were calculated for $Ra = 2.5 \times 10^7$ in the Cartesian geometry and are shown in Table 2. The 90% threshold suggested by Holmes is reached with the third eigenvalue for both parameters.

The first five modes are shown in Figure 11. These modes indicate that most of the variation in the system occurs near the center of the cavity. The structure of the modes is quantitatively similar to eigenmodes represented in prior work Liakopoulos *et al.* (1997). For $Ra = 2.5 \times 10^7$ the first five modes are used to calculate the temperature and streamfunctions of the system to visualize the error in using a reduced set of modes.

A higher Rayleigh number solution in the tri-cellular region was also analyzed. The modes are shown in Figure 12 and Table 2. The calculated temperature and streamfunction are shown in Figure 10. When compared with Figure 9 it is clear that key structures in the flow are not captured, specifically the third cell in the cavity center and the additional cell formation in the upper cavity (Π) and lower cavity ($4\Pi/8$). For complex fluid behavior in this region the POD does a relatively poor job even when 97% of the eigenvalue energy is used. The maximum differences are shown in Figure 8. In cases of very fine structure it may require retaining modes that represent as much as 99.5% of the total energy.

5. CONCLUSIONS

For natural convection with moderate driving force, COMSOL predicts the stable region of the flow and a transition to oscillatory flow as well as other computational tools do. The results for natural convection in a tall cavity with linear boundary conditions agree well with the results of Reeve *et al.* (2004) at low Rayleigh numbers. At higher Rayleigh numbers, the natural convection creates a multi-cellular flow pattern and temperature oscillations in the cavity.

These simulations over a wider Rayleigh number range show that the system transitions back to a stable oscillatory behavior as a third convection cell is formed in the cavity. The spectral analysis confirms that the system is undergoing a frequency doubling route to chaos following a supercritical Hopf bifurcation.

A POD analysis of this type has never been performed for this natural convection system. In general the 90% cumulative energy threshold for POD as suggested by other authors is not sufficient to characterize the flow or temperature structure of a system of this type. For the oscillatory region five modes were sufficient to reproduce key flow structures but at high Rayleigh numbers where the flow is more complex the POD was not able to capture the flow behavior. This indicates the need for a more robust approach to reduced order modeling for a system of this type. The limitations of POD in this problem may be reduced in part in future work by increasing the resolution of the CFD code in the time domain, but this change was not possible for consideration in the present work.

A traditional Galerkin projection was not calculated for this problem because of the dynamic system complexity. For example, if the $Ra = 2.5 \times 10^7$ results had been used as the base for a Galerkin projection it seems clear from examination of the modes that the $Ra = 18 \times 10^7$ would be poorly captured by the projection. In this case, future work based on the Galerkin projection outlined by Liakopoulos *et al.* (1997) will be modified for this problem. A projection will be derived for multiple Rayleigh numbers, representing the two cell, chaotic, and three cell regions of the flow. The authors believe that a Galerkin projection that crosses multiple Rayleigh numbers may be a robust way to represent the flow characteristics.

The POD results do provide an elegant method for understanding the complex flow behavior in the system. Future work may examine a wider Ra range for the annular geometry and additional radius ratios.

ACKNOWLEDGEMENTS

The authors wish to express sincere appreciation to the National Science Foundation for the principal funding of this work through Grant 0626533. Special thanks to Dr. Nathan Kutz, Matt Williams, Mikala Johnson and Chris Jones for technical review and mathematical suggestions.

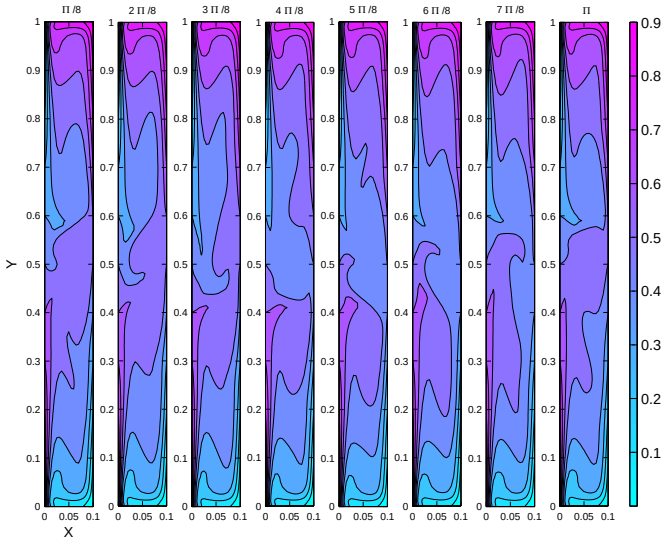

(a) Θ

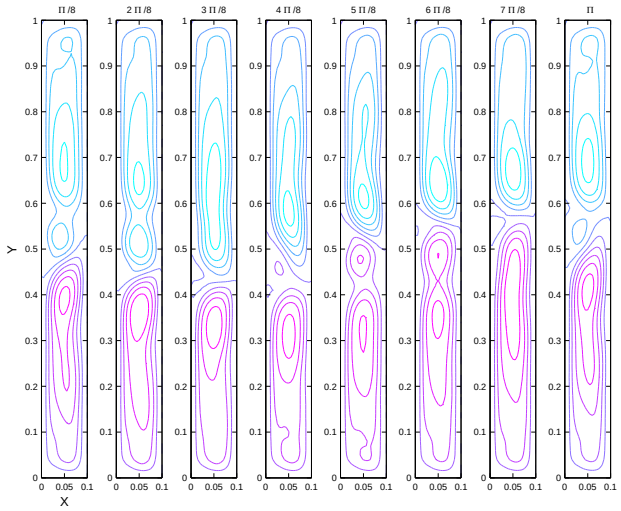

(b) ψ

Fig. 9 Sequential contour plot of the temperature Θ (upper) and stream function ψ (lower) for the rectangular cavity illustrating oscillation of the natural convection cells through one period (Π). $Ra = 17 \times 10^7$, $A = 10$.

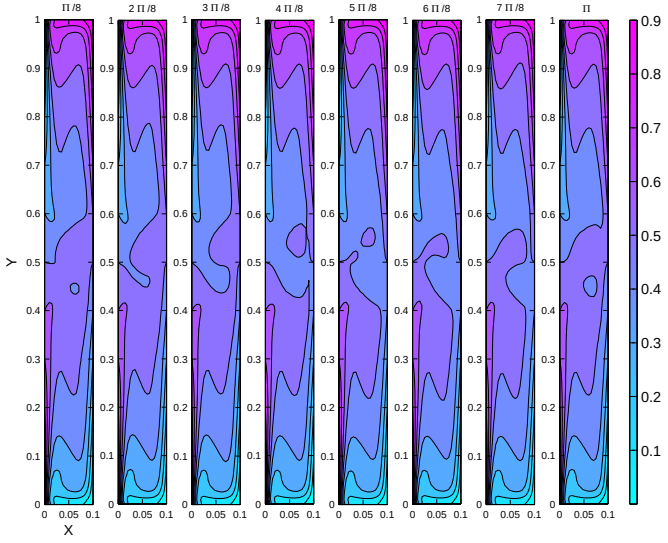

(a) POD Θ

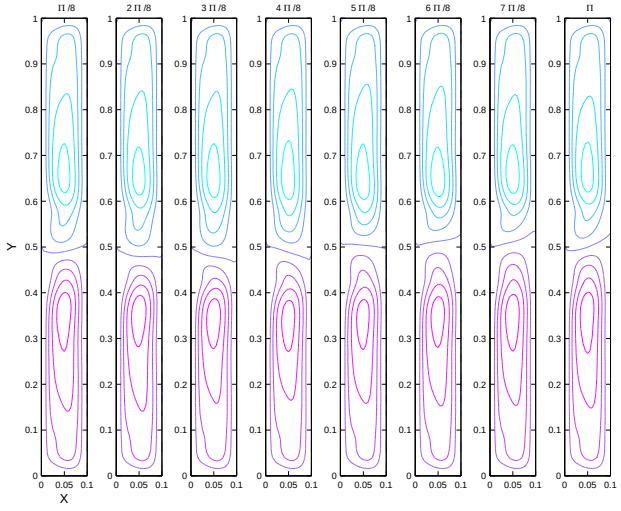

(b) POD ψ

Fig. 10 Temperature (a) and streamfunction (b) values calculated by the POD for $Ra = 17 \times 10^7$ with 5 modes. These should be compared with the computational results shown in Figure 9.

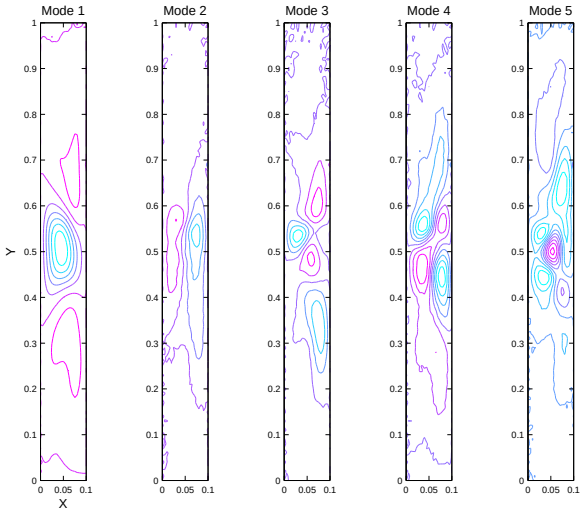

(a) Θ Modes

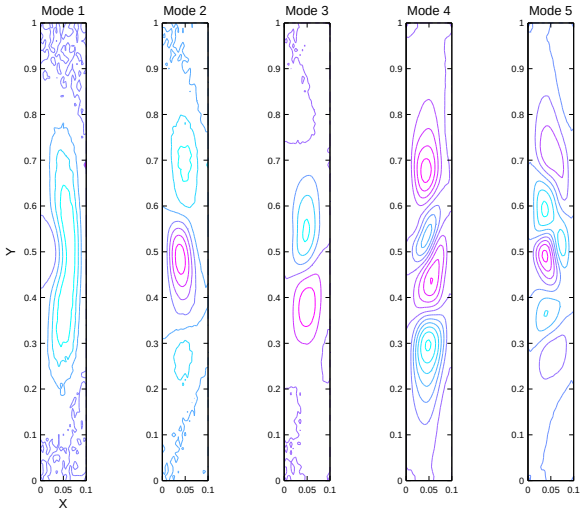

(b) ψ Modes

Fig. 11 Temperature (a) and streamfunction (b) modes calculated by the POD for $Ra = 2.5 \times 10^7$.

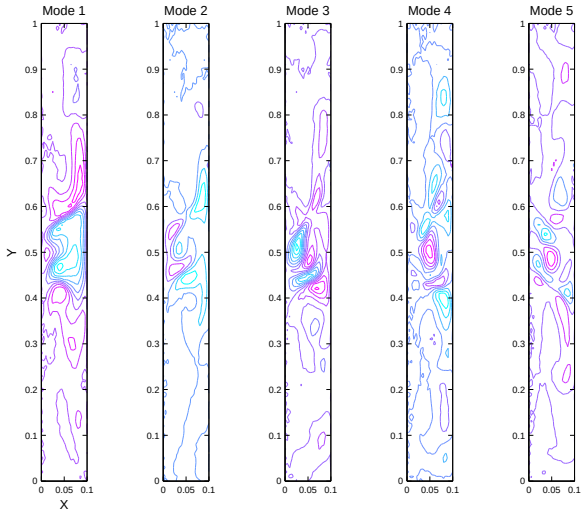

(a) Θ Modes

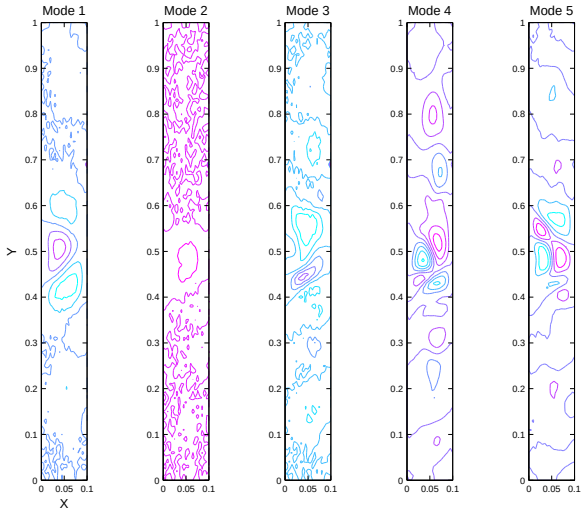

(b) ψ Modes

Fig. 12 Temperature (a) and streamfunction (b) modes calculated by the POD for $Ra = 17 \times 10^7$.

Global Digital Central
ISSN: 2151-8629

NOMENCLATURE

g	acceleration of gravity
H	height of the cavity
k	thermal conductivity
Pr	Prandlt number ($Pr = c_p\mu/k$)
Ra	Rayleigh number ($Ra = \frac{\rho^2 g c_p \beta(\Delta T) H^3}{k\mu}$)
p, P	dimensioned and dimensionless pressure
u, U	dimensioned and dimensionless velocity ($U = u/\sqrt{g\beta\Delta T H}$)
W	width of the cavity
Greek Symbols	
β	coefficient of thermal expansion
μ	dynamic viscosity
ρ	density
Θ	dimensionless temperature ($\Theta = \frac{T-T_c}{\Delta T}$)
t, τ	dimensioned and dimensionless time ($\tau = t\sqrt{g\beta\Delta T H^{-1}}$)

REFERENCES

Blinov, D., Prokopov, V., Sherenkovskii, Y., Fialko, N., and Yurchuk, V., 2004, "Effective Method for Construction of Low-dimensional Models for Heat Transfer Process," *International Journal Heat and Mass Transfer*, **47**, 5823–5828. http://dx.doi.org/10.1016/j.ijheatmasstransfer.2004.07.020.

Bonnet, J., Cole, D., Delville, J., Glauser, M., and Ukeiley, L., 1994, "Stochastic Estimation and Proper Orthogonal Decomposition: Complementary Techniques for Identifying Structure," *Experiments in Fluids*, **17**, 307–314.
http://dx.doi.org/10.1007/BF01874409.

Chait, A., and Korpela, S., 1989, "The Secondary Flow and Its Stability for Natural Convection in a Tall Vertical Enclosure," *Journal of Fluid Mechanics*, **200**, 189–216.
http://dx.doi.org/10.1017/S0022112089000625.

Chenoweth, D., and Paolucci, S., 1996, "Natural Convection in an Enclosed Vertical Air Layer with Large Horizontal Temperature Differences," *Journal of Fluid Mechanics*, **169**, 173–210. http://dx.doi.org/10.1017/S0022112086000587.

Dillon, H., Emery, A., Cochran, R., and Mescher, A., 2010, "Dimensionless versus Dimensional Analysis in CFD and Heat Transfer," *COMSOL User Conference*.

Dillon, H., Emery, A., and Mescher, A., 2009, "Benchmark Comparison of Natural Convection in a Tall Cavity," *COMSOL User Conference*.

Dillon, H., Emery, A., and Mescher, A., 2011a, "Chaotic Behavior of Natural Convection in a Tall Rectangular Cavity with Non-Isothermal Walls," *AIP Conference Proceedings*, vol. 1389, 127. http://dx.doi.org/10.1063/1.3636686.

Dillon, H., Emery, A., Mescher, A., Sprenger, O., and Edwards, S., 2011b, "Chaotic Natural Convection in an Annular cavity with Non-Isothermal Walls," *Frontiers in Heat and Mass Transfer*, **2**(2). http://dx.doi.org/10.5098/hmt.v2.2.3002.

Dillon, H., 2011, *Chaotic Natural Convection in an Annular Geometry*, Ph.D. thesis, University of Washington.

Haldenwang, P., and Labrosse, G., 1986, "2-D and 3-D Spectral Chebyshev Solutions for Free Convection at High Rayleigh Number," *Sixth International Symposium on Finite Element Methods in Flow Problems*.

Korpela, S., Gozum, D., and Baxi, C., 1973, "On the Stability of the Conduction Regime of Natural Convection in a Vertical Slot," *International Journal Heat and Mass Transfer*, **16**, 1683–1690. http://dx.doi.org/10.1016/0017-9310(73)90161-0.

Lee, Y., and Korpela, S.A., 1983, "Multicellular Natural Convection in a Vertical Slot," *Journal of Fluid Mechanics*, **126**, 91–121. http://dx.doi.org/10.1017/S0022112083000063.

LeQuere, P., 1990, "A Note on Multiple and Unsteady Solutions in Two-Dimensional Convection in a Tall Cavity," *Journal of Heat Transfer*, **112**, 965–974.
http://dx.doi.org/10.1115/1.2910508.

Liakopoulos, A., Blythe, P., and Gunes, H., 1997, "A Reduced Dynamical Model of Convective Flows in Tall Laterally Heated Cavities," *Proc R Soc London A*, **453**, 663–672.
http://dx.doi.org/10.1098/rspa.1997.0037.

Liakopoulos, A., Blythe, P., and Simpkins, P., 1990, "Convective Flows in Tall Cavities," *Simulation and Numerical Methods in Heat Transfer*, 81–87.

Paolucci, S., and Chenoweth, D., 1989, "Transition to Chaos in a Differentially Heated Vertical Cavity," *Journal of Fluid Mechanics*, **201**, 379–410.
http://dx.doi.org/10.1017/S0022112089000984.

Reeve, H., 2003, *Effect of Natural Convection Heat Transfer During Polymer Optical Fiber Drawing*, Ph.D. thesis, University of Washington.

Reeve, H.M., Mescher, A.M., and Emery, A.F., 2004, "Unsteady Natural Convection of Air in a Tall Axisymmetric, Non-isothermal Annulus," *Numerical Heat Transfer, Part A*, **45**, 625–648. http://dx.doi.org/10.1080/10407780490424262.

Rowley, C., 2005, "Model Reduction for Fluids, Using Balanced Proper Orthogonal Decomposition," *International Journal on Birfurcation and Chaos*.

Rowley, C., and Marsden, J., 2000, "Reconstruction Equations and the Karhunen-Loeve Expansion for Systems with Symmetry," *Physica D*, **142**, 1–19.
http://dx.doi.org/10.1016/S0167-2789(00)00042-7.

Sirisup, S., Karniadakis, G., Xiu, D., and Kevrekidis, I., 2005, "Equation-free/Galerkin-free POD-assisted Compuation of Incompressible Flows," *Journal of Compuational Physics*, **207**, 568–587. http://dx.doi.org/10.1016/j.jcp.2005.01.024.

Sirovich, L., 1987, "Turbulence and the Dynamics of Choerent Structures," *Quarterly of Applied Mathematics*, **45**(3), 561–590.

Suslov, S., and Paolucci, S., 1995, "Stability of Natural Convection Flow in a Tall Vertical Enclosure Under Non-Boussinesq Conditions," *International Journal of Heat and Mass Transfer*, **38**(12), 2143–2157. http://dx.doi.org/10.1016/0017-9310(94)00348-Y.

Trefethen, L.N., and Bau, D., 1997, *Numerical Linear Algebra*, Society for Industrial and Applied Mathematics.

Vest, C., and Arpaci, V., 1969, "Stability of Natural Convection in a Vertical Slot," *International Journal of Fluid Mechanics*, **36**, 1–15. http://dx.doi.org/10.1017/S0022112069001467.

Xin, S., and LeQuere, P., 2002, "An Extended Chebyshev Pseudo-Spectral Benchmark for the 8:1 Differentially Heated Cavity," *International Journal for Numerical Methods in Fluids*, **40**, 981–998. http://dx.doi.org/10.1002/fld.399.